Phd Thesis

M.C. Orlando Miguel Medina Cázares

July 16, 2014

Contents

List of Figures

Chapter 1

Regularized iterative least-squares algorithm for phase-shifting interferometry

1.1 Introduction

Phase Shifting Interferometry (PSI) demodulation methods are useful 1D temporal linear systems that allow us to recover the modulating phase of the PSI sequence. When the number of samples is small, typically between 3 and 15, we speak of PSI methods [1, 14], but they requiere a constant phase and do not tolerate missing data. On the other hand, when the number of samples is large, between 10^2 and 10^3, we speak of temporal analysis methods [7, 13, 3] which have many problems with the interferogram borders and missing data. Another possibility for analyzing the temporal signal is the use of a running PSI method tuned at the carrier frequency [7, 13, 3, 12, 11, 18]. For example if we use a tree step PSI method we could demodulate the phase locally for each of three consecutive samples. Although this method will deal well with borders, missing data cannot be handled and can even impede the use of this strategy. In experimental methods missing data appear in the case of a saturated signal and also in heterodyne temporal speckle-pattern interferometry when temporal decorrelation appears. Also missing data and discontinuities due to occlusions or shadows are very common in projected fringe profilometry. Besides these problems, noise is another important issue to solve; for example, in speckle techniques [1, 3] noisy interferograms are obtained, in consequence, recovered phase have to be treated to obtain a clean phase easy to unwrap.

Hence, in this paper we are going to present a full-field 2D linear demodulation method that uses in conjunction the temporal and spatial information in order to recover a clean phase, while interpolates empty small sections of missing data from the image space all with low computational time and in the same process.

1.2 Classical Least-Squares

Each (x, y) pixel of the PSI sequence is a 1D temporal discrete interferometric signal modeled in the following way,

$$\begin{aligned} I_{x,y}(k) &= a_{x,y} + b_{x,y}\cos(\phi_{x,y} + k\alpha) \\ &= a_{x,y} + c_{x,y}\sin(k\alpha) - s_{x,y}\cos(k\alpha), \end{aligned} \tag{1.1}$$

where $c_{x,y} = b_{x,y}\cos(\phi_{x,y})$ and $s_{x,y} = b_{x,y}\sin(\phi_{x,y})$ are the quadrature components of the 1D temporal interferometric signal, k is the discrete temporal variable, $a_{x,y}$ the background illumination, $b_{x,y}$ the modulation term, α the phase step or temporal carrier, and $\phi_{x,y}$ the modulating phase sought at the (x, y) pixel; note that all these variables are scalars. The independent temporal variable k represents the k-frame of the PSI sequence. In this context, knowing the temporal carrier α (phase step as known in PSI), the objective of the PSI demodulation methods is to estimate the quadrature components $c_{x,y}$ and $s_{x,y}$ of the interferometric signal at the (x, y) pixel. Then, the phase at (x, y) is obtained as:

$$\phi_{x,y} = \arctan\left(\frac{s_{x,y}}{c_{x.y}}\right). \tag{1.2}$$

Scanning all pixels in this way, we obtain the wrapped phase image of the PSI sequence. One of the first approaches to demodulate a PSI sequence was the least-squares model for PSI [10, 2, 4, 5]. The least-squares model (cost function) for PSI is the following,

$$U(a_{x,y}, c_{x,y}, s_{x,y}) = \sum_{k=0}^{N-1} \left[a_{x,y} + c_{x,y}\sin(k\alpha) \, - \, s_{x,y}\cos(k\alpha) - I_{x,y}(k)\right]^2, \tag{1.3}$$

where $I_{x,y}(k)$ is the observed value of the k-frame at the (x, y) pixel modeled as in Eq. (1.1). To have a well-posed mathematical model for Eq. (1.3), it is necessary to have at least three interferograms in the PSI sequence; that

is, $N \geq 3$. The parameters $c_{x,y}$ and $s_{x,y}$ that minimize Eq. (1.3) are the quadrature components used in Eq. (1.2) to obtain the phase. To minimize Eq. (1.3), we solve a 3×3 linear equation system where $a_{x,y}$, $c_{x,y}$ and $s_{x,y}$ are the unknowns. As the temporal interferometric signal of each pixel has the same model [see Eq. (1.1)], the solution of the linear equation system is always the same. This allows us to demodulate the interferogram sequence using very simple closed mathematical forms [1]. However, as shown in Eq. (1.3), this system never uses the spatial information but the temporal one; in fact, not one of the temporal PSI demodulation methods uses the spatial information [14]. Reason why, using temporal PSI demodulation methods we filter only through the interferogram sequence, but not through the interferogram image space. As a consequence, temporal PSI demodulation methods can not remove unwanted spatial harmonics or noise that may be introduced while recording the interferograms.

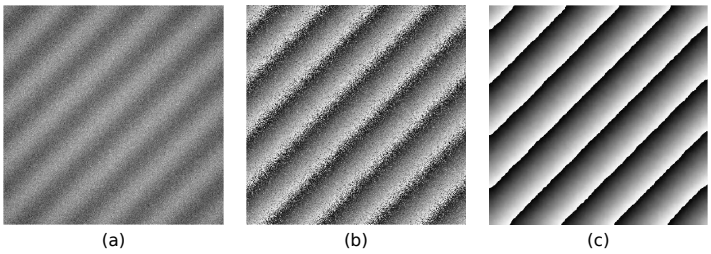

Figure 1.1: Numerical examples. a) One of four simulated interferogram sequences. b) Recovered phase map using classic least-squares. c) Recovered phase map using our proposed *Full-field 2D least-squares*.

1.3 Full-field 2D least-squares method

Regularization systems are very useful full-field systems that can use all the information needed to obtain the data sought as expected. In PSI, we can use these techniques to include the temporal and spatial information to recover the modulating phase as a smooth 2D function, removing unwanted harmonics and noise. Actually, regularization techniques have been used before in PSI for these purposes, the first were Marroquin et al. [7, 8, 9] and more recently others [15, 16, 6, 12, 17, 11, 18]. However, the approach used in those works obtained non-linear systems with a considerable computational work load. Besides, these algorithms need a pre-processing method

to remove background illumination in order to demodulate a correct phase. In our case, this preprocess is not needed and, also and more important, we will maintain the linearity of the least-squares cost function (1.3), adding spatial constraints to recover the wrapped modulating phase while removing noise and unwanted harmonics present in the interferograms [7], besides interpolating small sections of missing data. These constraints will penalize the spatial variations of the quadrature components $c_{x,y}$ and $s_{x,y}$ by using first order potentials as regularization terms. Proceeding in this way, the *Full-field 2D least-squares* cost function for PSI is the following:

$$\begin{aligned} U(\mathbf{a},\mathbf{c},\mathbf{s}) = & \sum_{k=0}^{N-1} \sum_{x,y\in L} \left[a_{x,y} + c_{x,y}\sin(k\alpha) - s_{x,y}\cos(k\alpha) - I_{x,y}(k)\right]^2 M_{x,y} \\ & + \lambda \sum_{x,y\in L} \left[(c_{x,y} - c_{x-1,y})^2 + (s_{x,y} - s_{x,y-1})^2\right] \\ & + \mu \sum_{x,y\in L} (a_{x,y} - a_{x-1,y})^2, \end{aligned} \tag{1.4}$$

where $M_{x,y}$ is a binary mask with valid measurement, λ is the regularization parameter that penalizes the spatial variations of quadrature components $\mathbf{c}$ and $\mathbf{s}$, and μ penalizes the spatial variations of background illumination $\mathbf{a}$. Note that in this case, the parameters $(\mathbf{a},\mathbf{c},\mathbf{s})$ of the cost function in Eq. (1.4) are scalar fields with dimensions $L_x \times L_y$ and elements $a_{x,y}$, $c_{x,y}$ and $s_{x,y}$, respectively, while the parameters $(a_{x,y}, c_{x,y}, s_{x,y})$ of the cost function in Eq. (1.3) are just scalars. As with the least-squares cost function of Eq. (1.3), here, at least three interferograms are needed in the sequence in oreder to have a well-posed mathematical model. To minimize Eq. (1.4), in order to obtain the quadrature components $\mathbf{c}$ and $\mathbf{s}$ that will give us the modulating phase, we need to solve a linear equation system of $3(L_x \times L_y)$ equations and $3(L_x \times L_y)$ unknowns. Compared with the 3×3 linear equation system of Eq. (1.3), the linear equation system of Eq. (1.4) is larger; however, solving this linear equation system is not so complicated when using numerical methods such as *Gauss-Seidel*. One of the advantages of the *Gauss-Seidel* method is that it is numerically stable, and it is not necessary to build the associated matrix of the linear equation system; besides, the *Gauss-Seidel* method can be programmed for today's modern parallel processors, such as the *Graphics Processing Unit* (GPU), speeding up the minimization process. For illustration purposes, in this paper we programmed the algorithm in *C++* language.

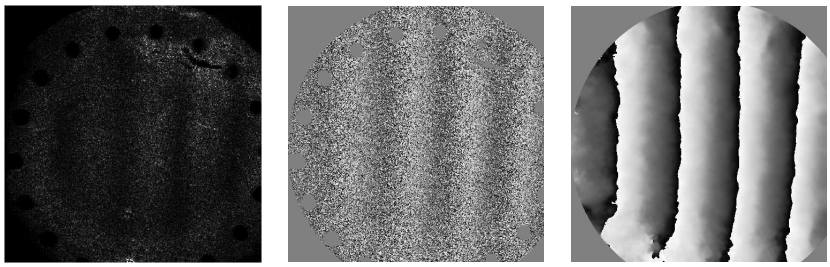

Figure 1.2: Experimental results. a) One of four experimental interferogram sequences. b) Recovered phase map using classic least-squares. c) Recovered phase map using our proposed *Full-field 2D least-squares*.

1.4 Numerical Experiments

To show the performance of the *Full-field 2D least-squares* algorithm, we simulated a PSI sequence of four interferograms of 512×512 pixels in the following way: $I_{x,y}(k) = a_{x,y} + b_{x,y}cos(\phi_{x,y} + k\alpha) + \eta_{x,y}$, for $k = 0, 1, 2, 3$ and $\alpha = \pi/2$. The modulated phase ϕ was modeled as a plane using the following expression: $\phi_{x,y} = 0.05x + 0.05y$. The background illumination term a was modeled as a parabola centered at pixel (256,256) of the image frames with a dynamic range between 0 and 1. The b term was set to 1. Last, we added a random field of white noise η, with mean $\gamma = 0$ and variance $\sigma^2 = 1$. In Fig. 1.1(a), we see the first interferogram of the simulated sequence. Figures 1.1(b) and 1.1(c) show the wrapped phase using classic least-squares [2] and the *Full-field 2D least-squares* method, respectively. To estimate the wrapped phase in Fig. 1.1(c), we solve the linear system in Eq. (1.4) using the Gauss-Seidel method and setting λ and μ to 50. The number of iterations was 500. For this example, the mask $M_{x,x}$ in Eq. (1.4) is one over all the image; since all the image it is valid information. Computational time was 4.6934 seconds, on a PC with an Intel Core i7 processor and 8 GB RAM memory . We can see in these figures that our proposed method recovers a phase with much less noise than the classic least-squares method, given the regularization terms in Eq. (1.4).

1.5 Experimental Results

Now, we are going to show the performance of our method with experimentally obtained interferograms and compare it qualitatively with the classical least-squares method. The interferogram sequence was generated using an ESPI technique, and the wave-front under test was modified applying pressure. For the phase step, a phase-shift of $\pi/2$ radians was introduced. The object under test was a circular metal plate with circular perforations all along its edge. In order to increase reflexion, we coated the plate with white powder, except for a small part, as can be seen in Fig. 1.2(a). Fig. 1.2(a) shows the first experimental phase-shifting interferogram of a 4 samples sequence. In Fig. 1.2(b), we show the wavefront estimation of the classic least-squares method, while in Fig. 1.2(c), we see the wave-front estimation of the *Full-field 2D least-squares* method proposed here. Computational time in this case was 7.6483 seconds using the PC described above. As we can see, the proposed method was able to estimate a phase free of noise. Another significant feature of this algorithm is that in sections where there is no information, such as black circles and scratches, the algorithm was able to fill-up the empty spaces satisfactorily; this is because it takes into account the neighboring pixel information and the regularization terms; very useful feature in the aforementioned cases.

1.6 Comments and conclusions

The calculation of a free-noise phase in PSI is very useful, since it allows us to use simple algorithms to unwrap the phase. Normally, to get a soft phase, we need to filter the interferogram samples or the output phase to remove the noise. The problem of this process is that we may be removing important information during the filtering. For this reason, the *Full-field 2D least-squares* algorithm represents a significant improvement to the classical least-squares method. Besides, as we have seen before, the presented algorithm is capable of interpolating small empty spaces of missing data, since it takes into account the temporal and spatial information. Therefore, all results presented in this paper can be directly applied to the spatial case where missing data and discontinuities are present. Examples of this are occlusions or shadows in projected fringe profilometry, temporal decorrelation and saturated signal in heterodyne temporal speckle-pattern interferometry.

Previous to this work, all phase-shifting algorithms only use a single pixel signal to estimate the wave-front under test, regardless of adjacent

information. This paper presents the usefulness of taking into account the temporal and spatial information in conjunction to estimate a best phase map. It is important to highlight that the functional of Eq. (1.4) is a linear system; therefore, it is stable and easy to compute. In conclusion, we present a full-field 2D linear demodulation algorithm able to recover a clean phase and also able to interpolate small empty sections of information, all with low computational time and in the same process.

Chapter 2

Regularized self-tuning phase demodulation for phase-shifting interferome try with arbitrary phase shifts

2.1 Abstract

In this work, we develop a regularization technique to demodulate a phase-shifting interferogram sequence with arbitrary inter-frame phase shifts. With this method, we can recover the modulating phase and inter-frame phase shifts in the same process. As all phase-shifting algorithms, the assumption is that the wavefront under test does not change over time but the phase-shifting introduction can vary in a non constant way. A notable characteristic of this demodulation method is that it not only can recover the modulating phase, but also it is capable of filtering-out large quantities of corrupting noise. We will show numerical experimental results and comparisons with other already published method to see the performance of the herein developed demodulation technique.

2.2 Introduction

Nowadays, Phase Shifting Interferometry (PSI) techniques are one of the most used techniques in optical metrology [1]. In PSI, one obtains an small sequence of at least 3 interferograms with a phase-shifting among them [1]. To recover the modulating phase there are standard demodulation PSI methods; the well known 3-, 4-, and 5-steps phase-shifting algorithms. Knowing the inter-frame phase-shifts (or temporal carrier) the standard methods recover the modulus 2π phase map with the minimum possible error [1**?** **?**]. If we do not know the phase-shifts exactly, we obtain a phase map with an unavoidable detuning error whose magnitude depends on the number of interferograms employed and how far we are from the actual phase-shifts [**?** **?** **?** **?** **?**]. This unfortunate case can occur when the optical interferometer setup is uncalibrated or perturbations from the environment affect the interferometer's optical path. For example, for most phase shifters such as a PZT there is a repeatability problem from hysteresis, non linearity, and temperature linear drift [**?** **?**]. Curiously, first phase-shifting algorithms where self-tuning nonlinear algorithms. Other approaches, propose error compensating algorithms to reduce detuning errors that basically use redundant data such as the Schwider-Hariharan 5-steps algorithm [**?** **?** **?**], and more recently by constructing a wide-band frequency response of the phase-shifting algorithm as the 7-steps algorithm shown in [**?**]. Further methods use the Fourier transform in order to estimate the inter-frame phase-shifts [**?** **?**], and other are based on the least-squares scheme estimating iteratively the inter-frame phase-shifts and phase [5**?**]. In Ref. 16[**?**], we presented an approach that estimates the local temporal carrier (the phase-shift) as the average of the phase difference between two consecutive phase maps obtained from two realizations of the tunable 3-steps algorithm. What we are going to show in this work, is a regularized self-tuning demodulation technique that obtains the analytical image (complex interferogram) and inter-frame phase-shifts from an interferogram sequence. Thus, we can recover the modulating phase modulus 2π and the inter-frame phase shifts in the same process. Here, it is not necessary to know the inter-frame phase-shifts. This inter-frame phase-shifts can vary arbitrary. The main difference between the demodulation method presented here, and the reported in [5**?** **?**], is that the herein demodulation method is based on a regularization technique that is able to remove noise from its input and is robust to non constant modulation variations, which is an issue that introduce errors in methods of works [5**?**]. Besides, we do not require estimate the fringe orientation as the method of work [**?**].

2.3 Method

In general, an interferogram sequence with arbitrary inter-frame phase-shifts can be modeled as

$$I_k(x,y) = a(x,y) + b(x,y)cos(\phi(x,y) + \alpha_k),\ k = 0,1,2,...,N-1, \quad (2.1)$$

where $I_k(x,y)$ is the intensity at the site (x,y) of the k-interferogram in a sequence of $N-1$ interferograms, being $a(x,y)$ its background illumination, $b(x,y)$ its contrast or modulation, $\phi(x,y)$ the modulating phase under test and α_k the phase-shifting of the k-interferogram. We can remove the background illumination of each interferogram in the following way:

$$I_k^{'}(x,y) = I_k(x,y) - [I_k * h](x,y),\ k = 0,1,2,...,N-1, \quad (2.2)$$

where $h(x,y)$ is the impulse response of a low-pass filter such as a Gaussian or mean filter and $*$ is the convolution operator[**?**]. Making this, the new interferogram sequence looks like

$$I_k^{'}(x,y) = b^{'}(x,y)cos(\phi(x,y) + \alpha_k),\ k = 0,1,2,...,N-1. \quad (2.3)$$

The main idea of the regularized self-tuning demodulation method that we show here comes from the article of Marroquin et al. [7]. The demodulation process presented by Marroquin et al., minimizes a nonlinear system that estimates the complex field of the first interferogram and its local spatial frequencies. We, unlike the Marroquin et al. work, estimate the inter-frame phase-shifts from the interferogram sequence. Therefore, our demodulation method minimizes the following quadratic functional

$$\begin{aligned} U(f,\alpha) &= \sum_{(x,y)} (\varphi(x,y) - I_0^{'}(x,y))^2 + \sum_{k=1}^{N-1} \sum_{(x,y)} [\frac{1}{2}[f(x,y)e^{i\alpha_k} + f^*(x,y)e^{-i\alpha_k}] - I_k^{'}(x,y)]^2 \quad (2.4) \\ &\quad +\lambda \sum_{(x,y)} [||D_x[f(x,y)]||^2 + ||D_y[f(x,y)]||^2],\ nonumber \quad (2.5) \end{aligned}$$

where $f = \{f(x,y) = \varphi(x,y) + i\psi(x,y) : (x,y) \in L\}$ is the complex field, $i = \sqrt{-1}$, and f^* its complex conjugated. The sums with the notation (x,y) underneath, runs over all valid sites (x,y) of the interferograms. Operators $D_x[]$ and $D_y[]$ takes the first order differences along x and y direction, as follows:

$$D_x[f(x,y)] = f(x,y) - f(x-1,y) + f(x,y) - f(x+1,y), \quad (2.6)$$

$$D_y[f(x,y)] = f(x,y) - f(x,y-1) + f(x,y) - f(x,y+1). \tag{2.7}$$

The regularization parameter λ controls the smoothness of the complex field [7, 9]. The first and second terms are the data terms, and the third term is the regularization term. Our reference is the first interferogram, therefore, we consider that its phase-shifting is $\alpha_0 = 0$. This is the reason of the first data term, which results when $k = 0$, and therefore, the second data term starts in $k = 1$. The minimization process of the functional (4) leads to a robust to noise nonlinear phase-shifting algorithm of N-steps that can recover the modulating phase and inter-frame phase shifts. With the complex field $\widehat{f}$ and phase-shifts α that minimize (4), the modulating phase is recovered as

$$\phi(x,y) = arg[\widehat{f}(x,y)] = arctan\left[\frac{\hat{\psi}(x,y)}{\widehat{varphi}(x,y)}\right]. \tag{2.8}$$

The minimization of functional (4), turns us to a nonlinear system that mathematically is impossible to solve by a direct numerical method. The dimension problem is m x n x N, where m x n is the interferogram dimension and N is the number of interferograms. For nonlinear systems, the iterative steepest-descent algorithm can converge to local minimums if its parameters are set adequately [**?**], but its converge speed results very slow in this case. Then, we split the problem in two: the linear part and the nonlinear part. The linear part are the equations that result by making zero the following partials: $\frac{\partial U}{\partial \varphi(x,y)}$ and $\frac{\partial U}{\partial \psi(x,y)}$, for all $(x,y) \in L$. The nonlinear part are the equations that result by making zero the following partial: $\frac{\partial U}{\partial \alpha_k}$, for $k = 0, 1, 2, ..., N-1$. Thus, to speed up the minimization process, our iterative minimization strategy combines in each iteration the Gauss-Seidel update for the linear part, and the steepest-descent update for the nonlinear part. Then, the iterations of our minimization strategy are given with the following updates:

$$\varphi^{n+1}(x,y) = Solve for \varphi^n(x,y) Eq.\left[\frac{\partial U(\ varphi^n + i\psi^n, \alpha^n)}{\partial \varphi(x,y)} = 0\right];\ \forall (x,y)\ in L \tag{2.9}$$

$$\psi^{n+1}(x,y) = Solve\ for\ \psi^n(x,y)\ Eq.\left[\frac{\partial U(\varphi^n + i\psi^n, \alpha^n)}{\partial \psi(x,y)} = 0\right];\ \forall (x,y) \in L \tag{2.10}$$

$$\alpha_k^{n+1} = \alpha_k^n - \mu \frac{\partial U(\varphi^n + i\psi^n,\ alpha^n)}{\partial \alpha_k},\ k = 0, 1, 2, ..., N-1. \tag{2.11}$$

Equations (8) and (9) correspond to the Gauss-Seidel update, and equation (10) is the steepest-descent update. In the appendix at the end of this paper, we show the explicit formulas of these equations. To see this implementation, the reader can download the source code following the web link of Ref. 22. Note: the provided source code of Ref. 22 is for illustration purposes, and it is no optimized as the C-language code used for our numerical experiments.

2.4 Numerical experiments and results

To obtain the results presented here, the minimization process described here made 1000 iterations to reach a relative convergence error of $1.322\,x\,10^{-4}$. This relative convergence error is calculated as $\sqrt{\sum(\alpha_k^n - \alpha_k^{n+1})^2}$, where the sum runs over $k = 1, 2, 3, ...N-1$, α_k^n is the k-phase-shift estimated in the current iteration and α_k^{n+1} is the k-phase-shift of the next iteration. This minimization process, coded and compiled in C-language, took a time of 11.310 seconds for these 512×512 interferogram frames in a computer with a 8-cores CPU of 1.73GHz having 8GB of memory RAM. The regularization parameter λ (see Eq. (4)) was set to $\lambda = 10$, and the parameter μ of the steepest-descent update was $\mu = \frac{1.2}{512x512}$ (see Eq. (10)). Actually, choosing $\mu = \frac{1.2}{512x512}$ is a very good parameter for the steepest-descent update of Eq. (10), where $m \times n$ is the dimension of the interferogram frames. In our numerical experiments, we start always the minimization process with initial values of $f = 0$, and $\alpha_k = k\frac{\pi}{2}$ for $k = 0, 1, 2..., N-1$. The interferogram sequence was generated as follows: The k-frame is given as $I_k = b(x,y)cos(\phi(x,y)+\alpha_k)+\eta(x,y)$, being $\eta(x,y)$ a random field of white noise with mean $\gamma = 0$ and variance $\sigma^2 = 4.84$ radians. The modulation, or contrast term $b(x,y)$, was modeled as a parabola centered at pixel $(256, 256)$ of the image frames with a dynamic range between 1 and 3. The inter-frame phase-shifts where generated as $\alpha_k = \pi + 0.4 * \varepsilon$, where ε_k is a random scalar with a uniform distribution between $-\pi$ and π radians. Here, we compare our results with the so called Advanced Iterative Algorithm (AIA) presented in Ref. [**?**] because this method estimates the phase and inter-frame phase-shifts as well, but using other approach. In Table. 1 , we show the errors values of the estimated phase-shifts using our regularized method and the estimated using the AIA method. This errors are calculated as $|\alpha_k - \alpha_k|$, where $\hat{\alpha}_k$ and α_k are the values of the estimated and actual phase-shifts for the k-frame, respectively. There we can see that our method estimates the inter-frame phase-shifts with less error. On the other hand, in Fig. 1 , we show the interferogram sequence and the recovered phase. Fig. 1.(A)

Steps	Proposed Method	AIA Method
0	0	0
1	0.0766	0.0904
2	0.0637	0.7146
3	0.0569	0.7083
4	0.0569	0.5520

Table 2.1: This table shows the error obtained between the phase-shift estimation and the actual phase-shift.

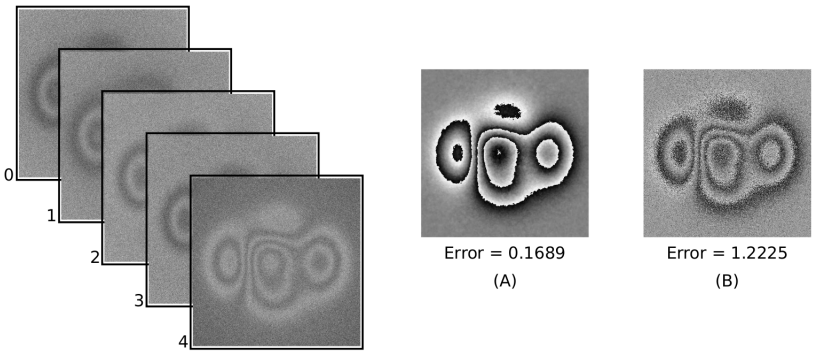

Figure 2.1: Interferogram sequence and the recovered phase. (A) shows the recovered phase and error using the regularized self-tuning method proposed here. (B) shows the recovered phase and error using the AIA method[15]. The error shown (in radians) is the standard deviation respecting the true phase map. The interferogram frames has a size of 512×512.

shows the recovered phase using the regularized self-tuning demodulation method presented here, while Fig. 1.(B) shows the recovered phase using the AIA method. We can see in this figure that our proposed regularized self-tuning demodulation method recovers the phase with less noise and error than with the AIA method. The errors shown in Fig. 1.(A) and Fig. 1.(B) are calculated as standard deviation of the difference between the recovered phase map and the true phase map used to generate the interferograms.

2.5 Conclusions

We have presented a regularized self-tuning phase-shifting demodulation method for interferogram sequences having arbitrary variations of the inter-frame phase-shifts. This method is robust to non constant spatial modulations. As shown in the results, our demodulation method is able to filter-out noise, and recover the modulating phase and the inter-frame phase-shifts with a minimum error. The demodulation method presented here is a non-linear demodulation method, however, we innovate the minimization strategy by mixing the steepest-descent update with the Gauss-Seidel update. In this way, we were able to speed up the minimization process and obtain the expected results.

APPENDIX

The iteration updates shown in Eqs. (8), (9) and (10) are given by taking the gradient of (4) and solving in the following way:

$$\varphi^{n+1}(x,y) = \frac{F_r(\varphi^n + i\psi^n, \alpha^n)}{H_r(\alpha^n)} \tag{2.12}$$

$$\psi^{n+1}(x,y) = \frac{F_i(\varphi^n + i\psi^n, \alpha^n)}{H_i(\alpha^n)} \tag{2.13}$$

where

$$\begin{aligned} F_r(\varphi^n + i\psi^n, \alpha^n) &= I_0(x,y) + \sum_{k=1}^{N-1}[I_k cos(\alpha) - \psi(x,y) sin(\alpha_k) cos(\alpha_k)] \\ &\quad +\lambda[\varphi(x-1,y)s(x-1,y) + \varphi(x+1,y)s(x+1,y) \\ &\quad +\varphi(x,y-1)s(x,y-1) + \varphi(x,y+1)s(x,y+1)], \end{aligned} \tag{2.14}$$

$$\begin{aligned} F_i(\varphi^n + i\psi^n, \alpha^n) &= \sum_{k=1}^{N-1} [I_k cos(\alpha) - \varphi(x,y) sin(\alpha_k) cos(\alpha_k)] \\ &+\lambda[\psi(x-1,y)s(x-1,y) + \psi(x+1,y)s(x+1,y) \\ &+\psi(x,y-1)s(x,y-1) + \psi(x,y+1)s(x,y+1)], \end{aligned} \tag{2.15}$$

$$H_r(\alpha) = \sum_{k=1}^{N-1} cos^2(\alpha_k) + \lambda[s(x-1,y) + s(x+1,y) + s(x,y-1) + s(x,y+1)] \tag{2.16}$$

$$H_i(\alpha) = \sum_{k=1}^{N-1} sin^2(\alpha_k) + \lambda[s(x-1,y) + s(x+1,y) + s(x,y-1) + s(x,y+1)] \tag{2.17}$$

The function $s(x_0, y_0)$ is an indicator function that is 1 if the point (x_0, y_0) is into the spatial domain of the interferograms, otherwise it is zero. Now, for the steepest-descent update (the phase-shifts α) the iteration update is:

$$\alpha_0^{n+1} = 0 \tag{2.18}$$

$$\alpha_k^{n+1} = \alpha_k^n - \mu \sum_{\forall (x,y) \in L} [\varphi^n(x,y) cos(\alpha_k^n) + \psi^n(x,y) sin(\alpha_k^n) - I_k(x,y)] \tag{2.19}$$

$$[\psi^n(x,y) cos(\alpha_k^n) - \varphi^n(x,y) sin(\alpha_k^n)]. \; nonumber \tag{2.20}$$

Note: suppose that α has the inter-frame phase-shifts that minimize (4). Its negative values minimize (4) as well. Then, while minimizing (4) it is possible obtain phase-shift values that looks different to the actual phase-shift values. This is not a problem, since we actually are interested in the modulating phase of the interferograms. However, it is always worth fix the inter-frame phase-shifts obtained in the following way:

$$\widehat{\alpha}_k = \begin{cases} \widehat{\alpha}_k & if \; |\widehat{\alpha}_k - \widehat{\alpha}_{k-1}| < \pi \\ \widehat{\alpha}_k - 2\pi & if \; \widehat{\alpha}_k - \widehat{\alpha}_{k-1} > \pi \\ \widehat{\alpha}_k + 2\pi & if \; \widehat{\alpha}_k - \widehat{\alpha}_{k-1} < -\pi \end{cases} \tag{2.21}$$

for $k = 1, 2, 3...N-1$, in order to have our inter-frame phase-shifts within the variation range$(-\pi, \pi)$.

Bibliography

[1] M. Servin D. Malacara and Z. Malacara. *Interferogram Analysis for Optical Testing*. Taylor & Francis, 2005.

[2] J. E. Greivenkamp. Generalized data reduction for heterodyne interferometry. *Optical Engineering*, 23(4):234350–234350–, 1984.

[3] Pascal Haible, Mahenda P. Kothiyal, and Hans J. Tiziani. Heterodyne temporal speckle-pattern interferometry. *Appl. Opt.*, 39(1):114–117, Jan 2000.

[4] A. Sato K. Okada and J. Tsujiuchi. Simultaneous calculation of phase distribution and scanning phase shift in phase shifting interferometry. *Opt. Commun.*, 84:118–124, 1991.

[5] In-Bok Kong and Seung-Woo Kim. General algorithm of phase-shifting interferometry by iterative least-squares fitting. *Optical Engineering*, 34(1):183–188, 1995.

[6] Ricardo Legarda-Saenz and Mariano Rivera. Fast half-quadratic regularized phase tracking for nonnormalized fringe patterns. *J. Opt. Soc. Am. A*, 23(11):2724–2731, Nov 2006.

[7] J. L. Marroquin, J. E. Figueroa, and M. Servin. Robust quadrature filters. *J. Opt. Soc. Am. A*, 14(4):779–791, Apr 1997.

[8] J. L. Marroquin, M. Servin, and R. Rodriguez-Vera. Adaptive quadrature filters and the recovery of phase from fringe pattern images. *J. Opt. Soc. Am. A*, 14(8):1742–1753, Aug 1997.

[9] J. L. Marroquin, M. Servin, and R. Rodriguez Vera. Adaptive quadrature filters for multiple phase-stepping images. *Opt. Lett.*, 23(4):238–240, Feb 1998.

[10] C. J. Morgan. Least-squares estimation in phase-measurement interferometry. *Opt. Lett.*, 7(8):368–370, Aug 1982.

[11] Julio C. Estrada Orlando Medina and Manuel Servin. Regularized self-tuning phase demodulation for phase-shifting interferometry with arbitrary phase shifts. *Proc. SPIE 8493, Interferometry XVI*, Sep 2012.

[12] Mariano Rivera, Rocky Bizuet, Amalia Martinez, and Juan A. Rayas. Half-quadratic cost function for computing arbitrary phase shifts and phase: Adaptive out of step phase shifting. *Opt. Express*, 14(8):3204–3213, Apr 2006.

[13] Pablo D. Ruiz, Jonathan M. Huntley, and Guillermo H. Kaufmann. Adaptive phase-shifting algorithm for temporal phase evaluation. *J. Opt. Soc. Am. A*, 20(2):325–332, Feb 2003.

[14] M. Servin, J. C. Estrada, and J. A. Quiroga. The general theory of phase shifting algorithms. *Opt. Express*, 17(24):21867–21881, Nov 2009.

[15] M. Servin, J. L. Marroquin, and F. J. Cuevas. Fringe-follower regularized phase tracker for demodulation of closed-fringe interferograms. *J. Opt. Soc. Am. A*, 18(3):689–695, Mar 2001.

[16] Manuel Servin, Jose Luis Marroquin, and Juan Antonio Quiroga. Regularized quadrature and phase tracking from a single closed-fringe interferogram. *J. Opt. Soc. Am. A*, 21(3):411–419, Mar 2004.

[17] J. Vargas, J. Antonio Quiroga, C. O. S. Sorzano, J. C. Estrada, and J. M. Carazo. Two-step interferometry by a regularized optical flow algorithm. *Opt. Lett.*, 36(17):3485–3487, Sep 2011.

[18] Fa Zeng, Qiaofeng Tan, Huarong Gu, and Guofan Jin. Phase extraction from interferograms with unknown tilt phase shifts based on a regularized optical flow method. *Opt. Express*, 21(14):17234–17248, Jul 2013.